Electronic Supplementary Material (ESI) for Physical Chemistry Chemical Physics.

Electronic Supplementary Information

Tunneling Effects in Confined Gold Nanoparticle Hydrogenation Catalysts

Leandro Luza,*[a] Aitor Gual,[b] Jesum Fernandes,[c] Dario Eberhardt,[d] and Jairton Dupont*[a]

[a]Laboratory of Molecular Catalysis, Universidade Federal do Rio Grande do Sul, Av. Bento Gonçalves, 9500, Porto Alegre, Brazil.

[b]Unitat de Tecnología Química (UTQ)-EURECAT, Centre Tecnològic de la Química de Catalunya (CTQC), c/ Marcel.lí Domingo, s/n, Building N5, Tarragona 43007, Spain.

[c]School of Chemistry, University of Nottingham, NG7 2RD, Nottingham, UK.

[d]PUCRS, Centro Interdisciplinar de Nanociências e Micro-Nanotecnologia, Av. Ipiranga, 6681, Porto Alegre, Brazil.

E-mail: leandro.luza@ufrgs.br; jairton.dupont@ufrgs.br.

Table of Contents

Section S1 3

1. Results and Discussion 3

1.1. Characterization of the Au-nanocatalysts 3

Section S2 12

2. Kinetic and Isotopic Experiments 12

Section S1

1. Results and Discussion

1.1. Characterization of the Au-nanocatalysts

^{13}C CP-MAS NMR analysis was performed to identify the characteristic signals of the immobilized ILs (Table S1 and Figure S1). The signals observed at 36 ppm were related to the methyl group substituent of the imidazolium ring whereas the signals at 11, 25 and 52 ppm were assigned to the propyl chain that connects the silicon atom to the imidazolium ring. Signals at 123 and 136 ppm were ascribed to the three imidazolium carbon atoms. The absence of any further carbon peak confirmed the presence of unreacted Si-C bonds, even under the acidic reaction conditions.

Table S1. ^{13}C CP-MAS NMR spectra data of the Au/*γ*-Al_2O_3, Au/**M1**, and Au/**M2** catalysts.

Catalyst	*δ* / ppm					
	(P1)	(P2)	(P3),(P4)	(P5)	(P6)	(P7)
Au/*γ*-Al_2O_3	—	—	—	—	—	—
Au/**M1**	36.5	136.7	123.3	52.2	25.1	10.7
Au/**M2**	35.5	136.4	122.8	52.2	24.8	11.0

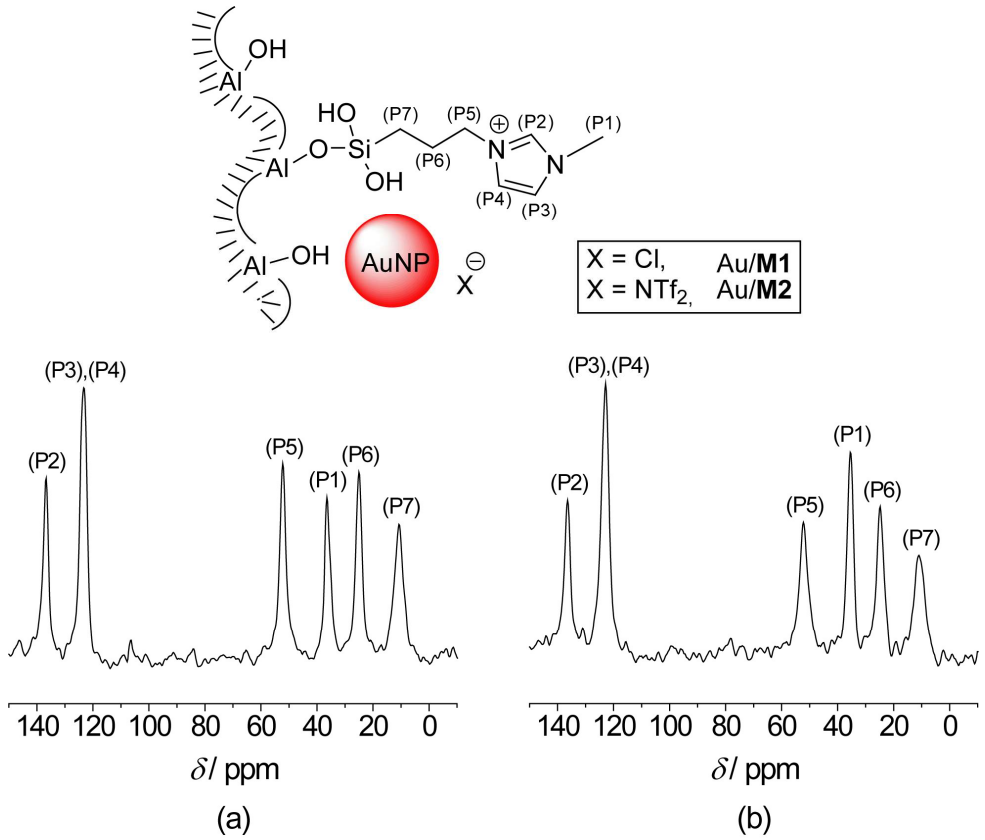

Figure S1. ^{13}C CP-MAS NMR spectra of the (a) Au/**M1** and (b) Au/**M2** catalysts.

The ^{29}Si CP-MAS NMR analysis was used to clarify the effect of the anion exchange step and to estimate the IL dispersion onto surface supports. Signals at −45 and −55 ppm attributed to T^1 (R*Si*(OAl)$(OH)_2$) and T^2 (R*Si*(OAl)(OSi)(OH)) species were observed for Au/**M1** and Au/**M2** catalysts with ratios of 16:84 and 24:67, respectively (Table S2 and Figure S2). After Cl^--exchange, it was observed the appearance of a third signal at −65 ppm (9%) assigned to the T^3 (R*Si*(OAl)$(OSi)_2$) species in the Au/**M2** catalyst.

Table S2. ^{29}Si CP-MAS NMR spectra data of the Au/γ-Al_2O_3, Au/**M1**, and Au/**M2** catalysts.

Catalyst	T^1	T^2	T^3
	δ/ ppm (Area/ %)	δ/ ppm (Area/ %)	δ/ ppm (Area/ %)
Au/γ-Al_2O_3	—	—	—
Au/**M1**	− 45 (16)	− 54 (84)	—
Au/**M2**	− 46 (24)	− 55 (67)	− 65 (9)

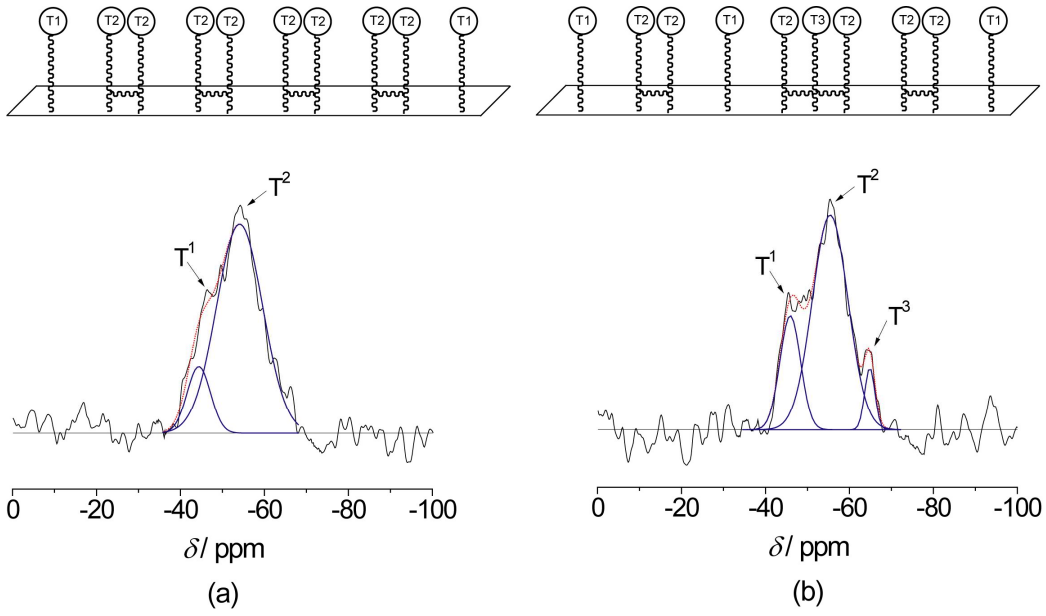

Figure S2. ^{29}Si CP-MAS NMR spectra of the (a) Au/**M1** and (b) Au/**M2** catalysts.

The FT-IR analysis of the catalysts revealed the characteristic bands of the ILs present on IL-hybrid aluminas (Table S3 and Figure S3). The signals at 1640 and 3460 cm^{-1} were assigned to the vibrations of the H_2O molecules adsorbed on catalysts. The characteristic bands about the stretching C−H of the imidazolium ring were observed at 3151 cm^{-1} and to the C−H of the alkyl groups at 1470, 2880, 2940 and 2970 cm^{-1}. The band at 1570 cm^{-1} is the characteristic stretching frequency of the C=N and C=C bonds present in the imidazolium ring. Furthermore, the FT-IR spectra of Au/**M2** catalyst displayed signals at 1064, 1207, 1332 e 1352 cm^{-1} attributed to NTf_2^- anion.

Table S3. FT-IR spectra data of the Au/γ-Al_2O_3, Au/**M1**, and Au/**M2** catalysts.

Attribution	Wavenumber/ cm^{-1}		
	Au/γ-Al_2O_3	Au/**M1**	Au/**M2**
ν (OH)	3460	3461	3470
ν (=C-H)	—	3151	3153
ν_{as} (C-H)[a]	—	2968	2972
ν_{as} (C-H)[b]	—	2941	2940
ν (C-H)	—	2882	2886
δ (H-O-H)	1639	1642	1635
ν (C=N)	—	1570	1565
ν (C=C)	—	1570	1565
δ (CH_2)	—	1470	1468
ν_{as} (SO_2)	—	—	1352
ν_{as} (SO_2)	—	—	1332
ν_{as} (CF_3)	—	—	1207
ν (S-N-S)	—	—	1064

[a] methyl group; [b] propyl chain.

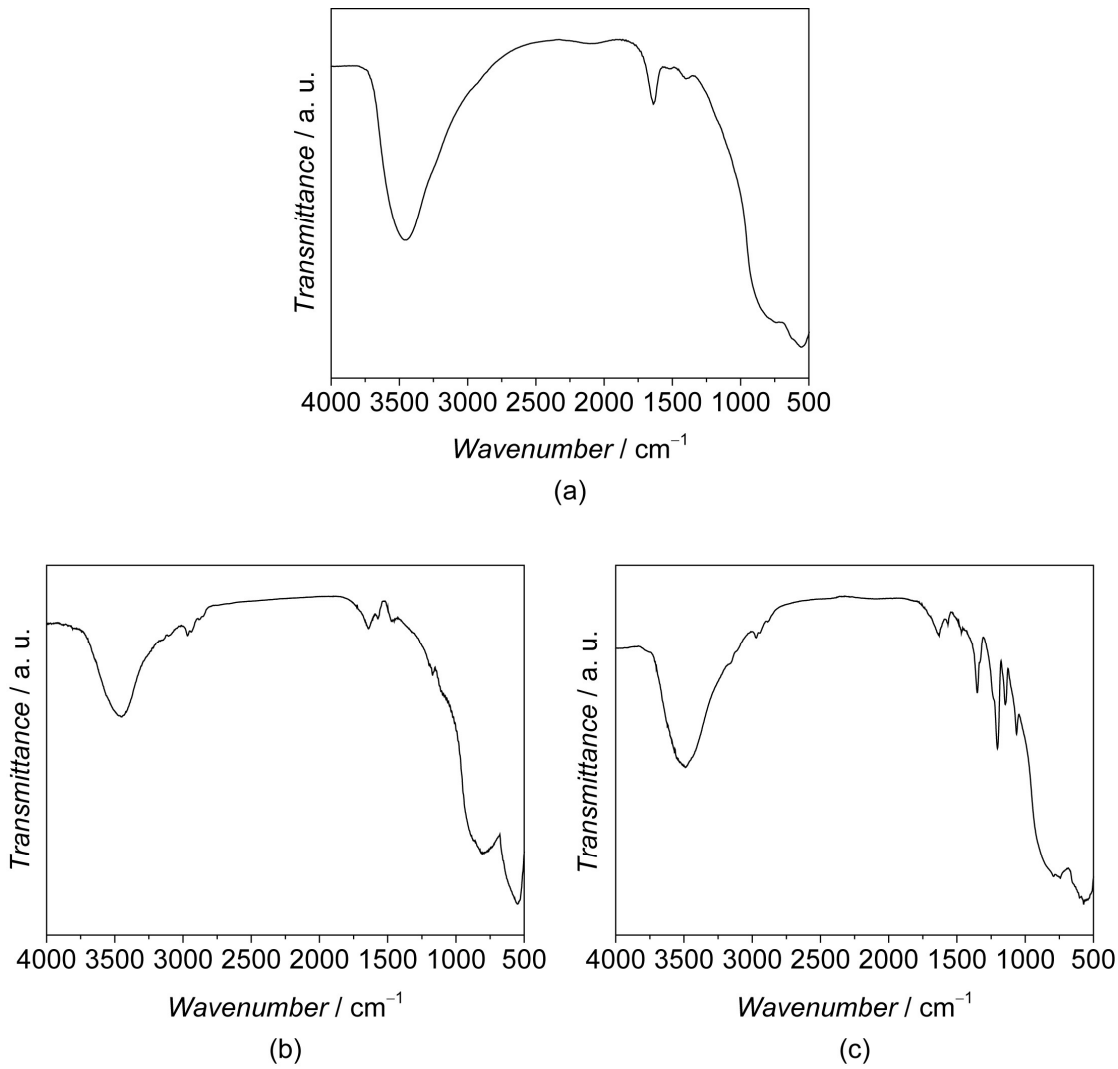

Figure S3. FT-IR spectra of the (a) Au/γ-Al_2O_3, (b) Au/**M1**, and (c) Au/**M2** catalysts.

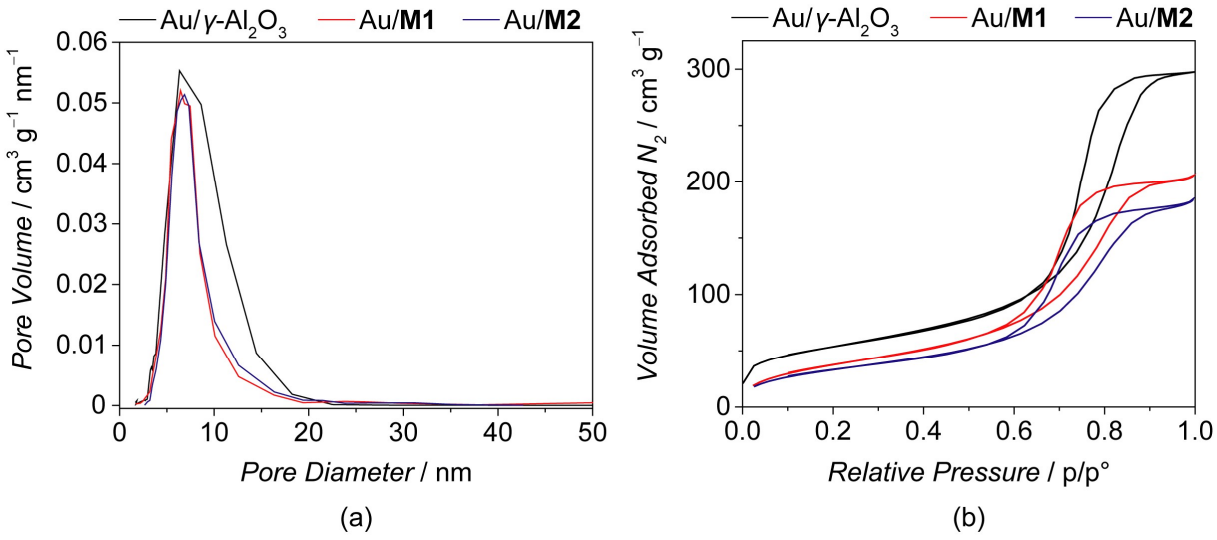

Figure S4. N_2-physisorption (a) BJH pore diameter distribution and (b) isotherms of the Au/γ-Al_2O_3, Au/**M1**, and Au/**M2** catalysts.

Table S4. Physical and chemical characteristics of the Au/γ-Al_2O_3, Au/**M1**, and Au/**M2** catalysts.

E.	Catalyst	IL[a]/ mmol g^{-1}	Au[b]/ wt.%	$\emptyset_{AuNPs}$[c]/ nm	S_{BET}[d]/ m^2 g^{-1}	$\emptyset_{Pore}$[d]/ nm
1	Au/γ-Al_2O_3	—	0.34 ± 0.05	6.6 ± 1.9	194	7.1
2	Au/**M1**	0.43	0.36 ± 0.04	6.8 ± 1.8	142	6.3
3	Au/**M2**	0.40	0.33 ± 0.03	6.4 ± 1.5	129	6.5

[a]Determined by CHN elemental analysis; [b]Determined by XRF analysis; [c]Determined by the Brunauer–Emmett–Teller (BET) multipoint method and Barrett-Joyner-Halenda (BJH) method; [d]Determined by TEM analysis.

RBS analysis showed that the amount of Au was much higher at the most external layers (~10 nm) of Au/γ-Al_2O_3, Au/**M1**, and Au/**M2** catalysts (Figure S5).

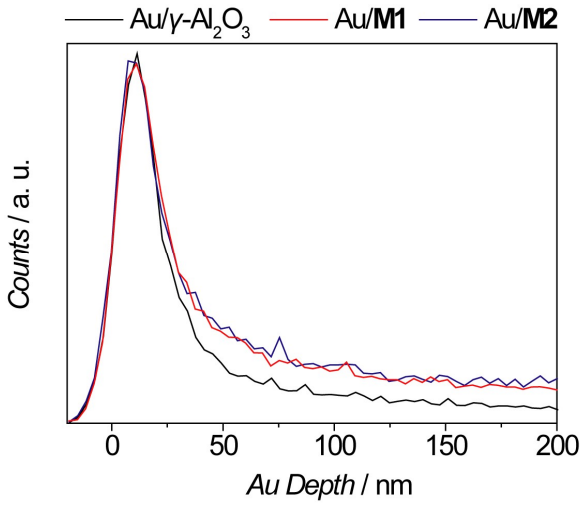

Figure S5. RBS depth-profile distribution for Au of the Au/γ-Al_2O_3, Au/**M1**, and Au/**M2** catalysts.

XRD and electron diffraction results revealed the characteristic pattern of the face-centered cubic (fcc) Au(0) lattice structure with typical diffraction peaks at 2θ angles of 38.2°, 44.1°, 64.5°, and 77.6°, corresponding to the (111), (200), (220), and (311) diffraction planes, respectively (Figure S6).

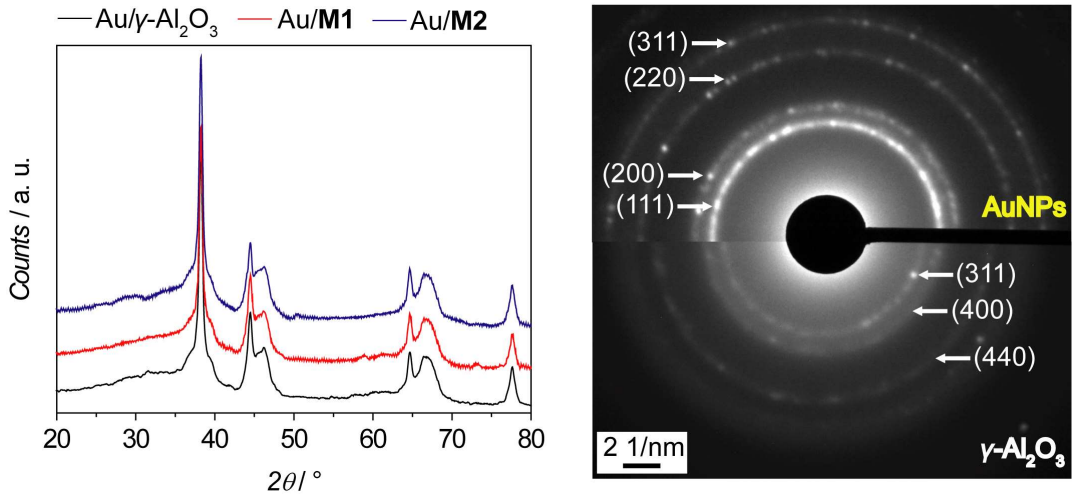

Figure S6. XRD patterns and electron diffraction of the Au/γ-Al_2O_3, Au/**M1**, and Au/**M2** catalysts.

In addition, TEM analysis exhibited well-distributed and small AuNPs on the Au/γ-Al_2O_3, Au/**M1**, and Au/**M2** catalysts with mean sizes of 6.6, 6.8, and 6.4 nm, respectively (Table S4 and Figure S7).

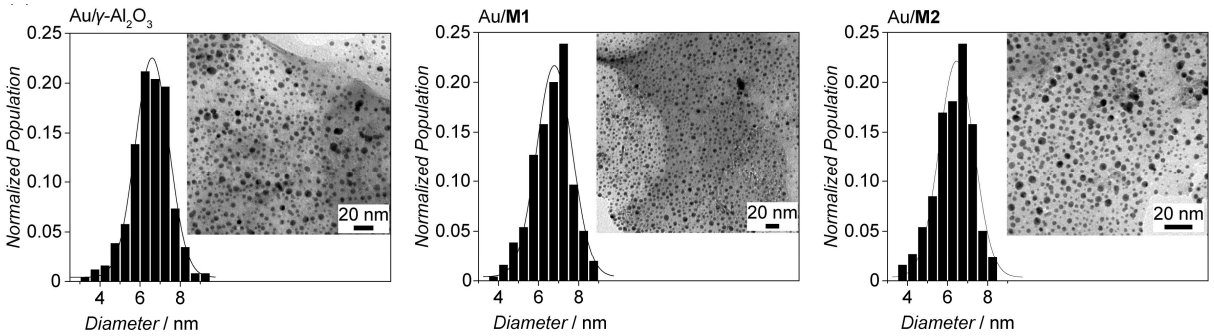

Figure S7. TEM images-size and histograms for Au on the Au/γ-Al_2O_3, Au/**M1**, and Au/**M2** catalysts.

Table S5. Composition *vs.* surface compositions of the Au/*γ*-Al_2O_3, Au/**M1**, and Au/**M2** catalysts.

E.	Catalyst	BE Au 4f[a]/ eV	IL:Au[b]/ (mol:mol)	Surface IL:Au[c]/ (mol:mol)	Al_2O_3:Au[b]/ (mol:mol)	Surface Al_2O_3:Au[d]/ (mol:mol)
1	Au/*γ*-Al_2O_3	84.0-87.7	—	—	566:1	1.4:1
2	Au/**M1**	83.7-87.4	22:1	1:9	536:1	1.3:1
3	Au/**M2**	83.7-87.5	24:1	1:7	584:1	1.5:1

[a]Determined by XPS analysis; [b]Calculated from the CHN elemental analysis and XRF analysis; [c]Surface composition calculated on the basis of the Au 4f and N 1s measured by XPS; [d]Surface composition calculated on the basis of the Au 4f and O 1s measured by XPS.

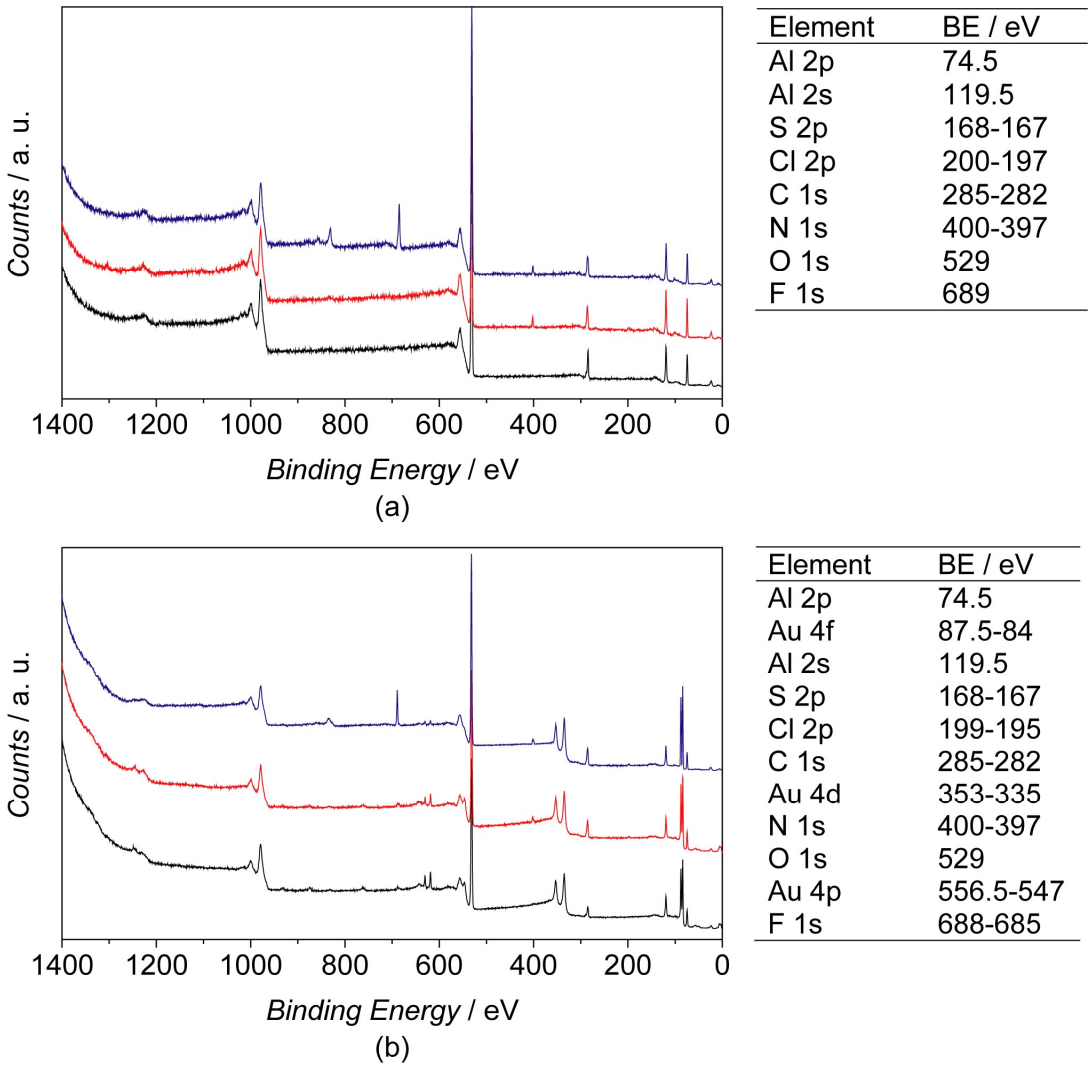

Figure S8. XPS at the long scan region of the (a) *γ*-Al_2O_3 (black), **M1** (red), and **M2** (blue) supports, and (b) Au/*γ*-Al_2O_3 (black), Au/**M1** (red), and Au/**M2** (blue) catalysts.

XPS analysis confirmed the effective exchange of chloride anions (Cl^-) by bis(trifluoromethane)sulfonimidate anions (NTf_2^-) on the IL-hybrid γ-Al_2O_3 **M2** support and, consequently, on the Au/**M2** catalyst (Figure S9).

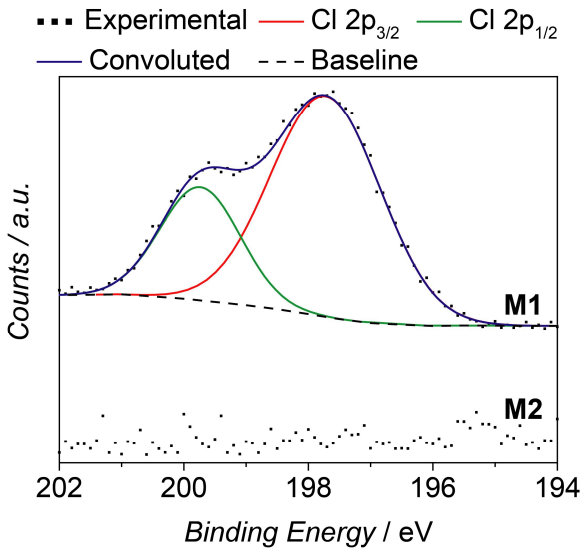

Figure S9. XPS measurements at Cl region of the **M1** and **M2** supports.

Section S2

2. Kinetic and Isotopic Experiments

Table S6. Reaction rates of the hydrogenation and deuteration of **1** catalyzed by Au/*γ*-Al_2O_3 at different temperatures.

Entry	$[\mathbf{1}]_0$	r_H and r_D / mmol L^{-1} h^{-1}				
		273 K	323 K	348 K	373 K	423 K
1	0.0125	0.6 and 0.6	1.1 and 0.3	2.7 and 1.0	4.3 and 1.9	6.2 and 3.8
2	0.025	1.3 and 0.9	3.6 and 1.6	5.4 and 3.1	9.2 and 3.6	11.7 and 8.1
3	0.05	2.6 and 1.5	5.8 and 2.9	8.4 and 4.9	14.4 and 6.2	21.8 and 15.1
4	0.1	4.3 and 2.3	12.2 and 6.3	17.2 and 10.6	28.6 and 11.5	37.8 and 26.3
5	0.2	5.6 and 3.8	16.5 and 9.6	27.1 and 17.1	46.8 and 20.9	70.6 and 49.5

[a]Reaction conditions: Au (0.5 μmol), anisole (10 mL), 2.5 MPa of H_2 or D_2, and 250 rpm; [b]Analyzed by gas chromatography (GC) and calculated at conversions of approximately 5%.

Table S7. Reaction rates of the hydrogenation and deuteration of **1** catalyzed by Au/**M1** at different temperatures.

Entry	$[\mathbf{1}]_0$	r_H and r_D / mmol L^{-1} h^{-1}				
		273 K	323 K	348 K	373 K	423 K
1	0.0125	0.2 and 0.05	1.7 and 0.7	3.0 and 2.1	3.4 and 2.9	4.5 and 3.6
2	0.025	0.3 and 0.1	2.6 and 1.3	5.9 and 4.3	6.3 and 5.0	10.3 and 8.3
3	0.05	0.6 and 0.2	3.8 and 1.9	10.2 and 7.4	12.4 and 9.8	17.5 and 14.1
4	0.1	1.1 and 0.4	7.7 and 3.7	19.5 and 14.1	21.4 and 16.9	31.2 and 25.1
5	0.2	1.3 and 0.5	11.5 and 5.6	31.9 and 23.0	38.5 and 29.9	59.2 and 46.8

[a]Reaction conditions: Au (0.5 μmol), anisole (10 mL), 2.5 MPa of H_2 or D_2, and 250 rpm; [b]Analyzed by gas chromatography (GC) and calculated at conversions of approximately 5%.

Table S8. Reaction rates of the hydrogenation and deuteration of **1** catalyzed by Au/**M2** at different temperatures.

Entry	$[\mathbf{1}]_0$	r_H and r_D / mmol L^{-1} h^{-1}				
		273 K	323 K	348 K	373 K	423 K
1	0.0125	0.2 and 0.06	1.1 and 0.6	1.9 and 1.3	2.1 and 1.6	2.6 and 2.2
2	0.025	0.3 and 0.1	2.1 and 1.0	3.7 and 2.4	3.9 and 3.1	6.3 and 5.5
3	0.05	0.6 and 0.2	2.8 and 1.3	6.5 and 4.2	7.6 and 5.9	10.8 and 9.4
4	0.1	1.1 and 0.3	5.8 and 2.8	12.2 and 8.0	13.2 and 10.3	19.1 and 17.0
5	0.2	1.3 and 0.5	8.7 and 4.3	20.2 and 13.1	24.0 and 18.2	36.6 and 31.6

[a]Reaction conditions: Au (0.5 μmol), anisole (10 mL), 2.5 MPa of H_2 or D_2, and 250 rpm; [b]Analyzed by gas chromatography (GC) and calculated at conversions of approximately 5%.

As the reaction rates of the hydrogenations and deuterations of *trans*-cinnamaldehyde (**1**) were dependent on the initial concentration of the substrate and zero order with respect to hydrogen and deuterium, we proposed that the *trans*-cinnamaldehyde (**1**) interacts with the AuNPs surface to form the adsorbed species which reacts with H_2 or D_2 to form the intermediate (hydroxyallyl for Au/*γ*-Al_2O_3 and 1-formylphenethyl for Au/**M1** and Au/**M2** catalysts) and the final product hydrocinnamaldehyde (**2**) (Scheme S2, see below). Thus, k_1 and k_4 are the kinetic constants for adsorption and k_{-1} and k_{-4} the kinetic constants for desorption of the substrate and product, respectively, and k_2 and k_3 the surface rate constants (combined into k_x, x = H or D). The RDS is the H_2 and substrate competitive adsorption/activation on the same active sites:

$$\mathbf{1} + * \underset{}{\overset{K_{1\text{-}x}}{\rightleftharpoons}} \mathbf{1}^*$$

$$\mathbf{1}^* \overset{K_2}{\rightleftharpoons} \textit{interm.}^*$$

$$\textit{interm.}^* \xrightarrow{k_3} \mathbf{2}^*$$

$$\mathbf{2}^* \overset{K_4}{\rightleftharpoons} \mathbf{2} + *$$

$$K_{1\text{-}x} = \frac{k_1}{k_{-1}} = \frac{[\mathbf{1}^*]}{[\mathbf{1}]\,[*]}$$

$$K_2 = \frac{k_2}{k_{-2}} = \frac{[interm.^*]}{[\mathbf{1}^*]}$$

$$K_4 = \frac{k_4}{k_{-4}} = \frac{[\mathbf{2}^*]}{[\mathbf{2}]\,[^*]}$$

$$r_x = k_3[interm.^*] = k_3K_2\,[\mathbf{1}^*] = \frac{k_xK_{1\text{-}x}[\mathbf{1}][^*]_0}{1 + K_{1\text{-}x}[\mathbf{1}] + K_4[\mathbf{2}]} \qquad \text{(Eq. S1)}$$

In this case, it is assumed that **2** is not adsorbed on the AuNPs surface in a kinetically significant amount and, thus, [**2**] >>> [**2***] leading to $K_4 \rightarrow 0$ and the following surface mass balance:

$$[^*]_0 = [\mathbf{1}^*] + [^*]$$

The total surface area of NPs normalized to the unit volume of the reaction medium ($[^*]_0$) is 0.427 $m^2\ L^{-1}$ and the rate of the reaction expressed by:

$$r_x = k_x[\mathbf{1}^*] = \frac{k_xK_{1\text{-}x}[\mathbf{1}][^*]_0}{1 + K_{1\text{-}x}[\mathbf{1}]} \qquad \text{(Eq. S2)}$$

with k_3 and K_2 combined into k_x as the overall surface reaction and intermediate adsorption.

Table S9. Adsorption parameters of the hydrogenation and deuteration of **1** by using the Au/*γ*-Al_2O_3, Au/**M1**, and Au/**M2** catalysts at different temperatures.

Entry[a]	T/ K	$K_{1\text{-}H}$[c]/ L mol^{-1}			$K_{1\text{-}D}$[c]/ L mol^{-1}		
		Au/*γ*-Al_2O_3	Au/**M1**	Au/**M2**	Au/*γ*-Al_2O_3	Au/**M1**	Au/**M2**
1	273	7.23	8.77	8.33	4.80	8.13	8.31
2	323	4.51	4.15	4.03	2.32	3.91	3.88
3	348	2.83	2.56	2.47	2.03	2.59	2.66
4	373	2.47	1.71	1.58	1.43	1.98	1.87
5	423	1.34	1.11	1.01	1.19	1.31	1.22

[a]Reaction conditions: Au (0.5 μmol), **1**/Au = (250-4000), anisole (10 mL), 2.5 MPa of H_2, and 250 rpm; [b]Rate constant normalized to the total surface area of the nanoparticles per unit of volume; [c]Determined by mathematical non-linear fitting of the experimental data.

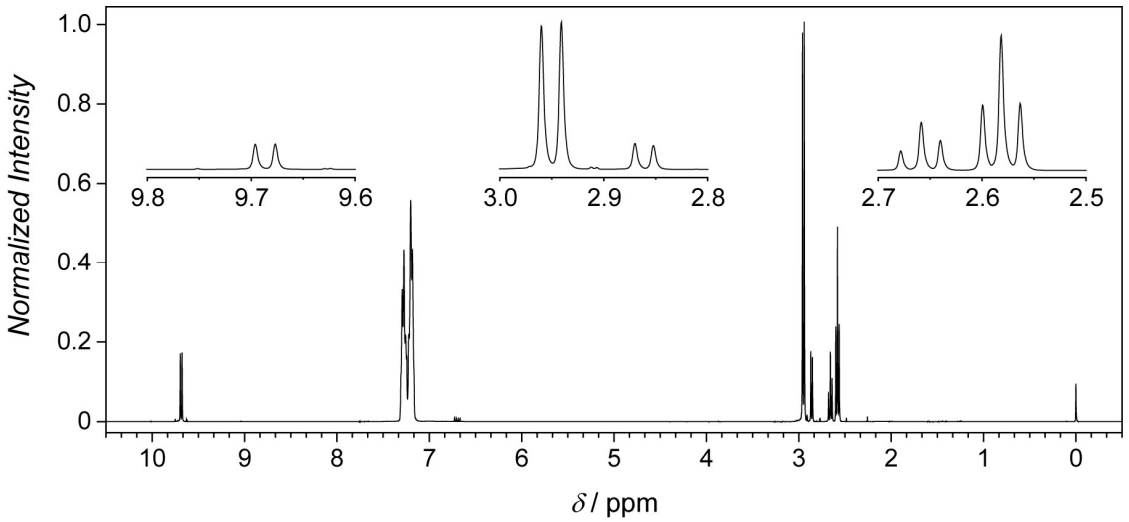

Figure S10. ^{1}H NMR spectra of the reaction products of the hydrogenation of *trans*-cinnamaldehyde with D_2 by using Au/*γ*-Al_2O_3 catalyst.

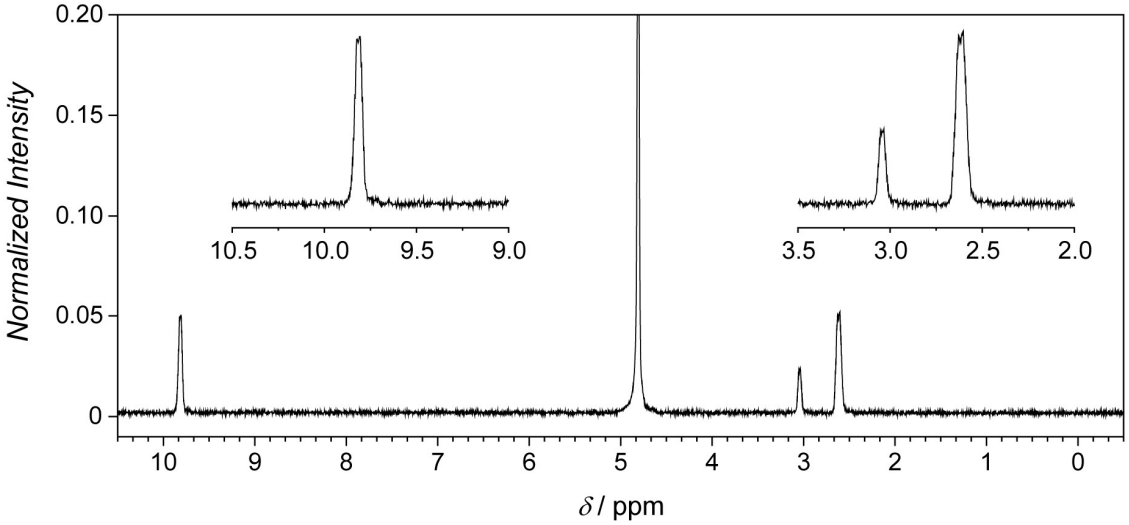

Figure S11. ^{2}H NMR spectra of the reaction products of the hydrogenation of *trans*-cinnamaldehyde with D_2 by using Au/*γ*-Al_2O_3 catalyst.

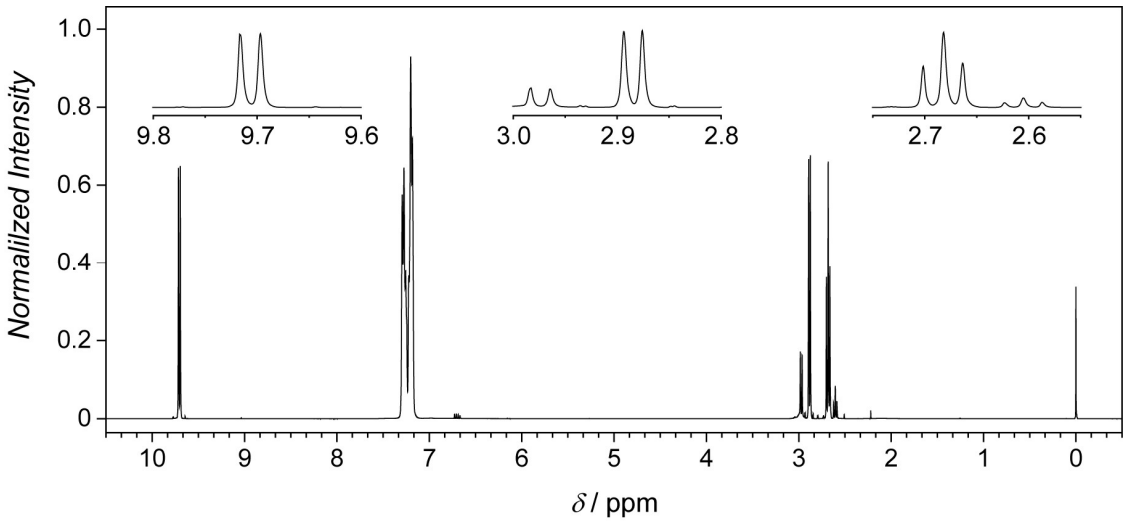

Figure S12. ^{1}H NMR spectra of the reaction products of the hydrogenation of *trans*-cinnamaldehyde with D_2 by using Au/**M1** catalyst.

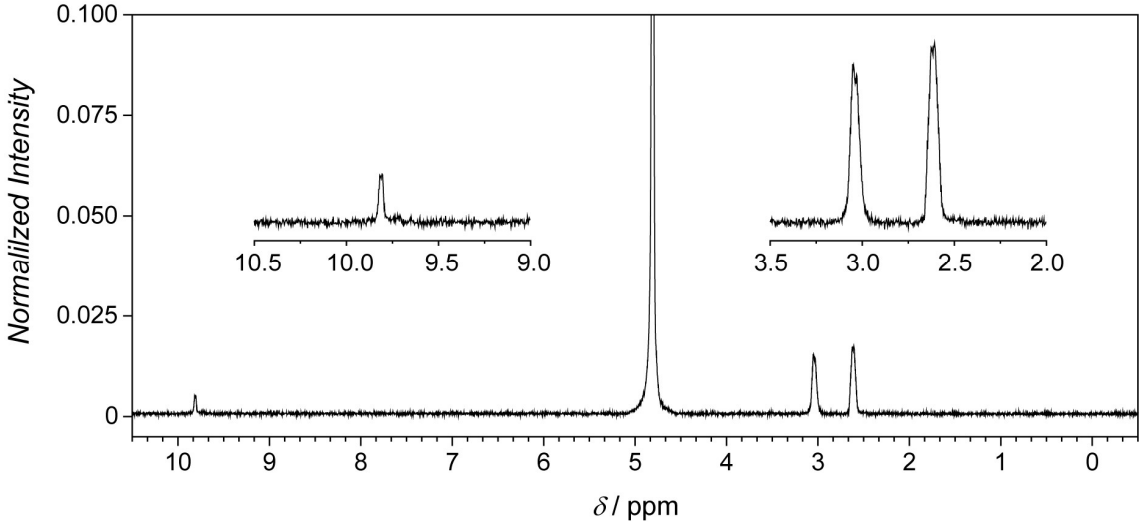

Figure S13. ^{2}H NMR spectra of the reaction products of the hydrogenation of *trans*-cinnamaldehyde with D_2 by using Au/**M1** catalyst.

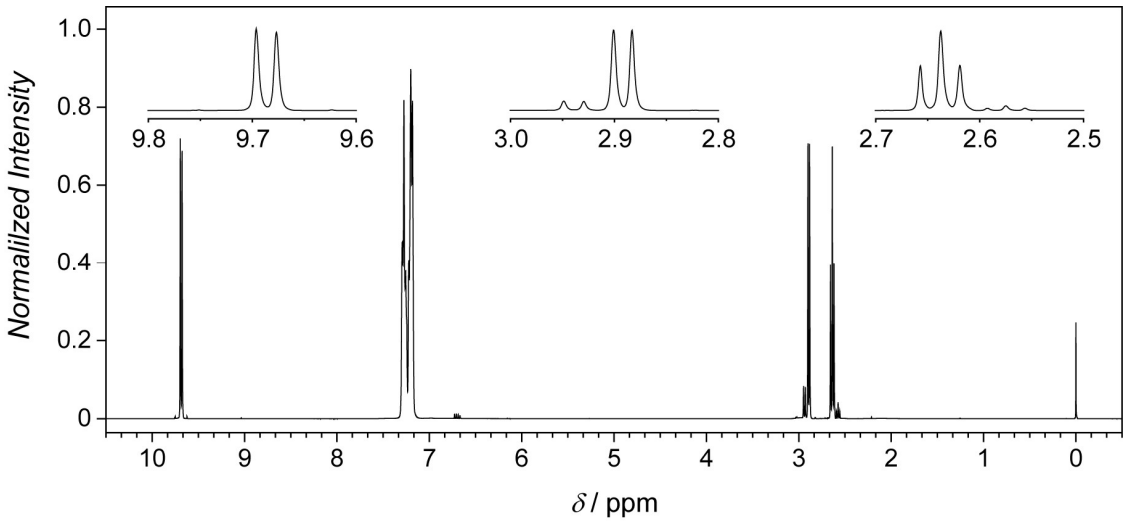

Figure S14. ^{1}H NMR spectra of the reaction products of the hydrogenation of *trans*-cinnamaldehyde with D_2 by using Au/**M2** catalyst.

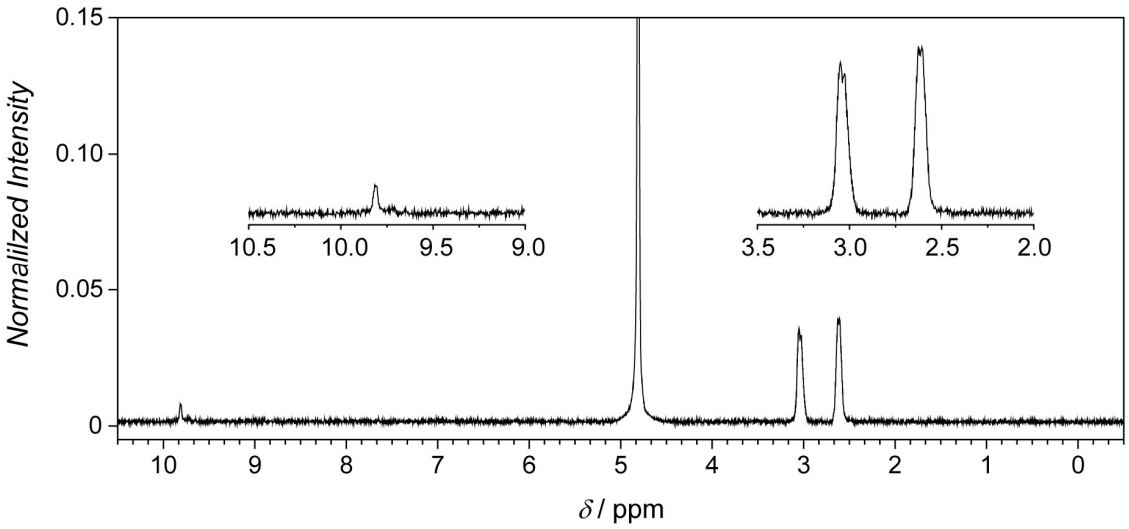

Figure S15. ^{2}H NMR spectra of the reaction products of the hydrogenation of *trans*-cinnamaldehyde with D_2 by using Au/**M2** catalyst.